Novel modification of Luminex assay for characterization of extracellular vesicle populations in biofluids

Olga Volpert (ovolpert@neurodex.co)
NeuroDex Inc.
Eve Gershun
NeuroDex Inc.
Katia Elgart
NeuroDex Inc.
Eren Erden
National Institute on Aging
Dimitrios Kapogiannis
National Institute on Aging
Ajay Verma
NeuroDex Inc.
Amir Levin
Columbia University
Vrinda Kalia
Columbia University
Haotian Wu
Columbia University
Andrea Baccarelli
Columbia University
Erez Eitan
NeuroDex Inc.

Article

Keywords:

Posted Date: June 28th, 2022

DOI: https://doi.org/10.21203/rs.3.rs-1723261/v1

Abstract

Most approaches to extracellular vesicle (EV) characterization are size based and provide few clues regarding EV origin, composition, and function. New methods to define EV surface proteins may aid understanding of their origin, physiological role, and biomarker potential. Recently developed highly sensitive immunoassays for intact EV using ELISA, NanoView, SIMOA and MesoScale platforms have limited multiplexing capabilities, whereas MACSPlex enables the detection of multiple EV surface proteins, but the requirement for large amounts of purified EVs limits its diagnostic usage. Here, we describe a Luminex-based immunoassay, which combines multiplexing capabilities with high sensitivity. The lack of enrichment and purification steps that makes it applicable to low sample volumes. We demonstrate assay's specificity for EV surface proteins via multiple EV depletion techniques, EV of known cellular origin, and by co-localization with established EV markers. Our novel approach elucidates the differences in tetraspanin profiles of neuronal and erythrocytic EV. Using size exclusion chromatography, we show that plasma EVs of neuronal origin differ in size from EV derived from erythrocytes, released by cutlured cells. In conclusion, our novel multiplexed assay differentiates between EV distinct tissue origins and has the potential to enable characterization of EV surface proteome and thus address EV molecular heterogeneity.

Introduction

Extracellular vesicles (EV) are released by all cells, via mechanisms including exocytosis, an outward budding of the plasma membrane and reverse-inward budding of endosomal membranes (Rak 2010; Colombo et al. 2014). Physical separation of EV subtypes presents a considerable challenge due to overlapping particle sizes and mass/flotation density, which contribute to extreme EV heterogeneity even in cell culture. In biofluids, such as plasma, EV heterogeneity is even more pronounced given distinctions in EV biogenesis and cellular origin. This in vitro and in vivo heterogeneity hinder the researchers' ability to ascribe functional roles to specific EV types. Since EV molecular composition closely mirrors cell(s) of origin (He et al. 2018) it is assumed that surface-exposed proteins also reflect differences between EV subtypes, including origin, biogenesis and function (Colombo et al. 2014). Using surface markers to define cell populations is a cornerstone of phenotypic and functional immunotyping. Although not proven, similar approach can be applied to EV typing, and better methodologies for surface protein detection are clearly desirable.

To address this issue, immunoassays were developed for intact EV cahracterization (Kanwar et al. 2014; Ohmichi et al. 2019; Ter-Ovanesyan et al. 2021), all based on a sandwich principle, wherein EV are captured and detected with an antibody pair against two distinct surface proteins (Fig. 1A). To generate a signal, both antigens should be interconnected, presumably via EV membrane, which requires colocalization on the same particle. This principle was incorporated into multiple platforms including traditional Enzyme-Linked Immunosorbent Assay (ELISA), MesoScale Discovery (MSD) electrochemiluminescence, Single Molecule Array (SIMOA), flow cytometry, Surface Plasmon Resonance (SPR) and many others. However, most of these methods provide limited capabilities for simultaneous examination of multiple proteins (Nolan and Duggan 2018; Chiang and Chen 2019; Kurian et al. 2021). One exception is MACSPlex FACS Exosome Kit (Miltenyi Biotech, cat. No 130-108-813), which enables detection of 37 EV surface epitopes. However, this arduous methodology requires EV enrichment prior to analysis and proficient, skilled operators.

Here, we describe Lumin-EX, the first intact EV immunoassay based on the Luminex platform (Fig. 1A). Lumin-EX utilizes MagPlex spheres routinely used by multiple assay manufacturers (Millipore-Sigma; R&D Systems). Our version enables sensitive simultaneous assessment of multiple EV surface markers and allows for the detection and in-depth analysis of specific EV populations in human plasma and in culture supernatants (EV profiling). This novel assay offers several key improvements in the balance of sensitivity and specificity, multiplexing capability, and ease of analysis. Moreover, Lumin-EX is optimized for the use with unprocessed plasma, an adjustment that simplifies the procedure, improves assay robustness and capacity for clinical use. Importantly, the use of unprocessed biofluids eliminates an added bias due to selective EV loss introduced by diverse isolation techniques.

Since the main principles of Lumin-EX and of flow cytometry are similar (Graham et al. 2019), we followed recently recommended instrumental and procedural controls for flow-based EV analysis (Welsh et al. 2020), including the demonstration of signal purge by EV depletion, a dilution-dependent signal reduction, and the lack of signal with the negative control capture or detection antibodies, as well as in unstained control. In agreement with previous findings (Thery et al. 2018), Lumin-EX showed distinct tetraspanin representation on the surface of plasma EV carrying distinct cell type markers. For example, CD9 was predominant on erythrocytic EV and underrepresented on EV positive for neuronal markers. In addition, Lumin-EX of plasma fractions generated by size exclusion chromatography (SEC) showed that EV carrying neuronal markers (GAP43, CD171) and EV positive for an erythrocytic marker CD235a segregate in distinct fractions, suggesting previously undocumented differences in size distribution.

In conclusion, Lumin-EX is a novel methodology, which incorporates Luminex platform to define EV surface protein composition, a sensitive and robust technique that supplements existing EV characterization methods and enables rapid and straightforward multifactorial analysis of EV surface proteins.

Materials And Methods

Preparation and characterization of Lumin-EX beads

Antibodies were conjugated to magnetic microspheres in selected color range, functionalized with carboxyl groups (MagPlex^{R}, Luminex Corp., Cat. No. MC1XXXX-01), using 1-Ethyl-3-(3-dimethylaminopropyl) carbodiimide (EDC) chemistry (He et al. 2007). Following conjugation, the resultant bead concentration (recovery) was determined in a Countess™ 3 FL automated cell counter (Thermo Fisher Scientific, Cat. No. A49866) using reusable chamber slides (Thermo Fisher Scientific, Cat. No. A25750). The beads were stored in a NeuroDex blocking buffer, which minimizes non-specific interactions, at a minimum concentration of $1x10^{6}$/ml and for up to 3 months. To measure antibody loading, Lumin-EX beads were resuspended in Assay Diluent at 5.010^{4} beads/ml and loaded into 96-well black plates (BrandTech, Cat. No. 781671), a minimum of 200 beads/well. Serially diluted PE-conjugated secondary antibodies were added in duplicate. Assay Diluent only was used as a background control. The staining was carried out for 30 min at room temperature in a Genie® Microplate Mixer (600 RPM). Beads were washed three times in a magnetic plate holder and resuspended in xMAP Sheath Fluid Plus (100 µl/well, Thermo Fisher Scientific, Cat. No. 4050021). The plates were analyzed in a Luminex 200 plate reader, a minimum of 100 beads per condition.

Preparation of biotinylated detection antibodies

Antibodies were biotinylated by overnight incubation at -4^{o}C with an EZ-link™ reagent (Thermo Fisher Scientific, Cat. No. 21442), at 20-fold molar excess, per manufacturer's instructions. Excess reagent was removed using Zeba™ Spin Desalting Columns, 7K MWCO (Thermo Fisher Scientific, Cat. No. 89882).

Lumin-EX procedure

sample where diluted (marked for each experiment) into a final volume of 50 µl in Assay Diluent and added into 96-well black plates. Assay Diluent only was used as a background control. Working suspension of Lumin-EX beads was generated to yield at least 2.5x10^{4} beads/ml for each antibody/bead combination, for up to 7 IEL analytes, and 50 µl of working suspension was added to each well. EV capture was carried out overnight (16–18 hours) at 4^{o}C on a microplate shaker (600 RPM). The plates were washed twice in a magnetic plate holder in NeuroDex Wash Buffer 1 and twice more in Wash Buffer 2, and the beads were resuspended in Assay Diluent supplemented with biotinylated detection antibody (1-2 µg/ml, 50 µl/well). After 2 hours incubation at room temperature, in a microplate shaker, the beads were washed 3 times in Wash Buffer 2, resuspended in 50 µl PBS supplemented with Streptavidin-PE reagent (SAPE, 6 µg/ml) and incubated 20 min at room temperature, with shaking. Following SAPE incubation, the beads were washed 3 times in Wash Buffer 2, resuspended in xMAP Sheath Fluid, and analyzed in a Luminex200 plate reader.

Size exclusion chromatography

EVs from cell culture conditioned media were concentrated in a 100kDa MWCO Amicon spin filter (EMD Millipore, Cat. No. UFC910096), and plasma EVs were concentrated by precipitation with an optimized PEG reagent (NeuroDex). The concentrated samples (0.5 and 2 ml, as appropriate) were subjected to size exclusion chromatography (SEC) using pre-calibrated columns (IZON Science, qEV Original, 35 nm and qEV2, 35 nm for conditioned media and plasma, respectively). Void volume and up to 25 fractions (0.5 and 2.0 ml, respectively) were collected, and protein concentration (A280 absorption) was measured using NanoDrop2000 spectrophotometer (Thermo Fisher Scientific).

EV isolation from conditioned media

Media conditioned by induced pluripotent stem cell (iPSC)-derived neurons was purchased from BrainXell. iPSCs had been differentiated into cortical neurons using BrainXell proprietary protocol. Serum-free conditioned media (120 ml total) were collected over 4 weeks, with 50% of the media collected each week. HEK293 cells were grown in a medium supplemented with 10% FBS; at 50–70% confluence, the media was replaced with EV-free, serum-free basal media, and the cells were incubated for additional 48 hours. The media were cleared by two centrifugation rounds (10 min, 3,000xg), and EV were collected by ion exchange chromatography (IEC) on Q Sephadex as described previously (Kosanovic et al. 2017). The unbound material was washed with excess equilibration buffer (0.05 M Tris–HCl, pH 7.6), followed by step elution in 0.05 M Tris–HCl, pH 7.6, supplemented with 0.25M NaCl to remove weakly bound proteins and with 0.5 M NaCl for total EV elution. Finally, the EV were concentrated by dialysis against NeuroDex storage buffer supplemented with protease and phosphatase inhibitors (Thermo Fisher Scientific, Cat. No 78429, 78426) in 100 kDa MWCO spin filters.

Transmission Electron Microscopy

EV suspensions (four ml per sample, fresh or fixed overnight, in 1% paraformaldehyde) were loaded onto glow-discharged copper mesh Formvar-coated carbon grids (Sigma-Aldrich, Cat. No G4776) and allowed to adsorb for ~ 30s. The grids were briefly washed in ddH_2O, stained with 2.5% aqueous Uranyl Acetate solution, and allowed to fully dry on air before imaging. Grids were imaged using a FEI Morgagni transmission electron microscope (FEI, Hillsboro, OR) operating at 80 kV and equipped with a Nanosprint5 CMOS camera (AMT, Woburn, MA).

Detergent treatment of crude EV fractions

Crude EV fractions generated by PEG-based precipitation (plasma EVs) or by centrifugation/ultrafiltration through 100 kDa MWCO Amicon spin filter (Millipore UFC901008) were supplemented with Triton X-100 to a final 2% w/v concentration and incubated for 1–2 hours at room temperature or for 30 min at 50^{o}C.

RNA isolation and amplification

For RNA isolation, SEC fractions 2–5 and 9–14 were pooled and concentrated using 100kDa MWCO Amicon filters. RNA was isolated with the miRNeasy serum/plasma kit (Qiagen, Cat. No 217184) following the manufacturer's instructions with minor modifications (RNase-free DNase treatment). cDNA was generated using SuperScript™ VILO™ cDNA Synthesis Kit (Thermo Fisher Scientific, Cat. No: 11754050) following manufacturer's instructions. For mRNA TaqMan kit and primers (Thermo Fisher Scientific, Cat. No. 44-445-56 and 4331182) see Table 3.

Lipidomic analysis

Lipidomic profiling was performed by Ultra Performance Liquid Chromatography-Tandem Mass Spectrometry (UPLC-MSMS). Lipid extracts were prepared from live microsomes by a modified Bligh and Dyer method (Bligh and Dyer 1959), spiked with appropriate internal standards, and analyzed using Agilent 1260 Infinity HPLC in an Agilent 6490A QQQ mass spectrometer controlled by MassHunter V 7.0 (Agilent Technologies, Santa Clara, CA). Glycerophospholipids and sphingolipids were separated by normal-phase HPLC as described previously (Chan et al. 2012), using an Agilent Zorbax Rx-Sil column (2.1 x 100 mm, 1.8 µm) at 25°C. In a combination of mobile phase A (chloroform: methanol: ammonium hydroxide, 89.9:10:0.1, v/v) and mobile phase B (chloroform: methanol: water: ammonium hydroxide, 55:39:5.9:0.1, v/v) phase A was maintained at 95% for 2 min, decreased linearly to 30% over 18 min, further decreased to 25% over 3 min, then restored to 95% over 2 min and maintained for 6 min. Separation of sterols and glycerolipids was carried out on a reverse-phase Agilent Zorbax Eclipse XDB-C18 column (4.6 x 100 mm, 3.5mm) with an isocratic mobile phase, chloroform, methanol, 0.1 M ammonium acetate (25:25:1) at a flow rate of 300 µl/min.

Lipid species were quantified by multiple reaction monitoring (MRM) transitions (Hsu et al. 2004; Guan et al. 2007; Chan et al. 2012) using positive and negative ionization modes together with referencing of appropriate internal standards: PA 14:0/14:0, PC 14:0/14:0, PE 14:0/14:0, PG 15:0/15:0, PI 17:0/20:4, PS 14:0/14:0, BMP 14:0/14:0, APG 14:0/14:0, LPC 17:0, LPE 14:0, LPI 13:0, Cer d18:1/17:0, SM d18:1/12:0, dhSM d18:0/12:0, GalCer d18:1/12:0, GluCer d18:1/12:0, LacCer d18:1/12:0, D7-cholesterol, CE 17:0, MG 17:0, 4ME 16:0 diether DG, D5-TG 16:0/18:0/16:0 (Avanti Polar Lipids, Alabaster, AL). To calculate lipid content for each sample, the sums of the number of moles of all species measured by all three LC-MS methodologies were normalized to mol %. The final data are presented as mean mol % ± S.E.M.

Results

Lumin-EX allows specific detection of EV surface proteins in unprocessed plasma. We generated Lumin-EX (LMX) beads for the following surface antigens: CD9, an EV marker; CD68, a macrophage marker; purinergic receptor P2RY12, a microglia marker, and neuronal marker axonal protein GAP43 (see Table 1for capture antibodies). All antibodies were loaded at 0.5, 1.0, 2.0 and 5.0 µg/ml, with bead concentration below $5x10^6$/ml. Antibody loading was assessed by staining with serially diluted PE-conjugated secondary antibodies (Table 2) and measured in a Luminex200 reader (Thermo Fisher Scientific). Figure 1B shows CD9 loading. For further bead production, we used antibody concentrations at the higher end of a linear range, where mean fluorescence intensity (MFI) increased in proportion to the antibody concentration prior to saturation (1–5 µg/ml).

Table 1
Capture and detection antibody for intact EV Luminex

Antigen	Vendor	Cat. No.	Host/Type	Species specificity	Marker specificity
CD9	BioLegend	312102, 312112	Mouse Monoclonal	human, simian	Pan-EV
CD63	BioLegend	353039, 353018	Mouse Monoclonal	human, simian	Pan-EV
CD81	BioLegend	349502, 349514	Mouse Monoclonal	human, simian	Pan-EV
CD171	Thermo Fisher Scientific	14-1719-82	Mouse Monoclonal	human	Neuronal, gut
CD235a	BioLegend	349502	Mouse Monoclonal	human	Erythroid cells
GAP43	Thermo Fisher Scientific	MA5-32256	Rabbit monoclonal	Human, mouse, rat	Neuronal
P2RY12	BioLegend	848002	Rat Monoclonal	Mouse, human	Microglia

Table 2
secondary antibody to control IEL bead loading

Antibody	Vendor	Cat. No.
PE Goat anti-mouse IgG	BioLegend	312102
PE Donkey anti-rabbit IgG	BioLegend	406421
PE Goat anti-rat IgG	BioLegend	405406

LMX beads generated as in Fig. 1A were tested for EV detection in unprocessed, serially diluted plasma from healthy donors (BioIVT), using a cocktail of biotinylated tetraspanin antibodies for detection (CD9, CD63, and CD81, pan-TSPN; see Table 3 for detection antibodies). The analysis of two random unprocessed plasma using LMX beads appended with antibodies against specific targets generated strong dose-dependent signals with a

linear range between 10 and 50 µl plasma input corresponding (Fig. 1C, D). In contrast, LMX beads loaded with an isotype-matched IgG (a negative control) generated low signal, likely representative of non-specific EV adherence (Fig. 1B, C). To ascertain that the signal can be specifically attributed to plasma EV, EV were depleted prior to analysis using PEG-based precipitation or detergent lysis (Triton-X100, 2% final concentration). In both cases, the signal was reduced by ~ 80% (Fig. 1E). Finally, to demonstrate the specific capture of intended antigen(s), we used culture media conditioned by HEK293 cells overexpressing neuronal antigens GAP43 or CD171 (L1CAM; see Methods). Figure 1F shows that CD171-positive EV are captured by the LMX beads appended with CD171 but not with GAP43 antibodies. Conversely, EV from the media conditioned by GAP43-overexpressing cells were captured with GAP43 and not with CD171 beads (Fig. 1G). Together, our results show that Lumin-EX detection is EV-specific, antigen-specific and applicable for small volumes of unprocessed human plasma or conditioned media.

Table 3
Primers used in the study

Gene transcript	Gene ID	Vendor	Cat. No.
Neurogranin (NRGN)	Hs00382922_m1	Thermo Fisher Scientific	4331182
SRY-Box Transcription Factor 1 (SOX1)	Hs01057642_s1	Thermo Fisher Scientific	4331182
Oligodendrocyte Transcription Factor 1 (OLIG1)	Hs00744293_s1	Thermo Fisher Scientific	4331182
Oligodendrocyte Transcription Factor 2 (OLIG2)	Hs00300164_s1	Thermo Fisher Scientific	4331182
Hypocretin/Orexin (HCRT)	Hs01891339_s1	Thermo Fisher Scientific	4331182
Glyceraldehyde-3-Phosphate Dehydrogenase (GAPDH)	Hs02786624_g1	Thermo Fisher Scientific	4331182
Platelet Factor 4 (PF4)	Hs00427220_g1	Thermo Fisher Scientific	4331182
Heterozygous Beta-Globin/ Hemoglobin (HBB)	Hs00758889_s1	Thermo Fisher Scientific	4331182

Lumin-EX capture results in minimal cross-populational contamination. Using capture beads targeting specific EV populations, e.g., erythrocyte- or neuron-derived, we were able to demonstrate minimal cross-reactivity between antigens specific for diverse cell types. Specifically, EV captured with beads decorated with antibodies against neuronal marker GAP43 were detected with high sensitivity using the pan-TSPN cocktail, GAP43 and CD171 antibodies (Fig. 1H) but not with antibodies against macrophage (CD68) and erythrocyte (CD235) markers. Similarly, beads appended with CD171 antibody (neuronal marker) captured EV population detectable with pan-TSPN cocktail and with antibody against another neuronal marker, GAP43. A modest signal upon CD68 detection is consistent with low-level CD171 expression on circulating monocytes (Fig. 1I). Conversely, EV population captured with CD235 beads was detectable only with pan-TSPN and CD235 antibodies, while lacking positivity for GAP43, CD171 and CD68 (Fig. 1J) and EV captured with CD68 beads were detected only with pan-

TSPN, CD68, and to a low degree, CD171 antibodies (Fig. 1K), due to a minimal L1CAM expression on macrophages.

Lumin-EX is suitable for multiplexed assessment of EV surface proteins. The foremost advantage of the Luminex platform is its multiplexing capacity. To show Lumin-EX equally suitable for multiplexed measurements, we compared the sensitivity of multiplexed and single-bead Lumin-EX assays for tissue-specific and ubiquitous EV surface markers, including erythrocyte marker CD235 (Glycophorin A), macrophage marker CD68, pan-EV markers CD63 and CD81, and neuronal markers GAP43 and CD171. A dose-dependent signal reduction was shown for each analyte, with a clear linear range between 10–50 µl plasma input (Fig. 2A). To assess the potential sensitivity loss due to multiplexing, we generated dose/response curves for each analyte in single-bead and multiplexed assays. In both cases, the resultant dose-response curves showed linearity within similar input ranges (Fig. 2B-F). Consistent with findings by others, CD9 measurement in 25 random plasma samples revealed significant differences between individual donors; however, single-bead and multiplexed assays showed strong correlation (Fig. 2G).

Interestingly, analysis of matched human sera and plasma showed a predominance of erythrocytic EV in the serum, to the exclusion of other signals (see Supporting Information).

Lumin-EX informs co-localization of EV surface molecules. To analyze potential differences in the EV surface proteome from distinct cellular origins, we used several permutations of the capture beads and detection antibodies. The use of neuron-specific GAP43 capture beads with either pan-TSPN or GAP43 detection antibodies (Fig. 3A) resulted in similar signal strength, suggesting that most GAP43 is EV-associated. Interestingly, when GAP43 capture beads were combined with either CD9, or CD63, or CD81 detection, CD9 antibodies produced a significantly weaker signal (Fig. 3B), suggesting that CD63 and CD81 are the two predominant tetraspanins on GAP43-positive neuronal EV. Interestingly, EV released by the cultured neuronal cells, but not by HEK293 also showed lower signal with CD9 detection, compared CD63 and CD81 (Fig. 1H-K and data not shown). In contrast, EV captured with CD235 beads were efficiently detected with CD9, but not with CD63, nor CD81 antibodies (Fig. 3C), suggesting that CD9 is a dominant tetraspanin on CD235-positive erythrocytic EV. These differences in tetraspanin presentation between EV populations suggest that the differences in Lumin-EX signal cannot be attributed solely to the differences in antibody affinity, but rather stem from populational differences in surface presentation of specific antigens. Our observations are consistent with earlier findings [reviewed in (Thery et al. 2018; Witwer and Thery 2019)], e.g., high CD9 expression on erythrocytic EV. Furthermore, EV captured with CD9 beads were strongly positive for CD235, while GAP43 detection generated only a modest signal (Fig. 3D), and EV captured with CD63 or CD81 beads showed weaker positivity with CD235, compared to GAP43 detection (Fig. 3E, F). Together, these results demonstrate that Lumin-EX is useful for characterization and co-localization analysis of EV markers, with the goal of identification and quantitative detection of EV populations.

Lumin-EX of SEC fractions uncovers cell-specific size differences in plasma EV

To further characterize Lumin_EX assay, it was used to examien the fractions generated by SEC of human plasma. Concentrated plasma EV (see methods) were loaded onto pre-calibrated qEV columns (IZON Sciences) and all fractions including void volume collected and analyzed. To detect EV-specific signals, we used pan-TSPN detection cocktail combined with a variety of capture beads including CD9, CD235, CD68, GAP43 and CD171. The combination of CD9 beads and pan-TSPN detection produced the expected signal that peaked between fractions 2–5 and trailed to fraction 9 (Fig. 4A). CD235 capture and pan-TSPN detection showed a narrow peak

in fraction 3 suggestive of a tighter size range (Fig. 4B). Unexpectedly, capture with the beads appended with antibodies against either a macrophage marker CD68, or one of the two neuronal markers, GAP43 and CD171, upon pan-TSPN detection, yielded strong signals in the fractions 11–18, 8–15 and 11–18, respectively (Fig. 4C-E), suggesting smaller particle sizes. Similar results were obtained using LMX beads for the kidney marker, Podocin (See Supporting Information). In agreement, TEM analysis of pooled early (2–5) and late (8–14) fractions (qEV Original, IZON Sciences) showed spherical particles 75–125 nm in diameter in fractions 1–6 and particles ranging between 15 and 40 nm in diameter in fractions 8–14 (Fig. 4F).

To characterize the TSPN-positive signal in late fractions, we repeated the analysis, using GAP43 capture beads followed by pan-TSPN detection or detection with individual TSPN antibodies (Fig. 5A-D). Consistent with the analysis of unprocessed plasma above, pan-TSPN detection yielded strong positive signals in fractions 7–15, (Fig. 5A), largely attributable to CD63 and CD81, since the CD9 detection alone resulted in a weak (< 50 net MFI) positive signal in fractions 11–16 and CD63 and CD81 detection yielded much stronger signals (Fig. 5C, D). In agreement, CD9 capture followed by GAP43 detection produced a weak signal in fractions 10–16, while CD63 and CD81 capture followed by GAP43 detection yielded stronger signals in fractions above 10.

To ascertain whether the late-fraction signal detected with pan-TSPN cocktail is attributable to EV, in accordance with MISEV guidelines (Thery et al. 2018; Welsh et al. 2020), crude EV preparation was subjected to detergent pre-treatment to disrupt the plasma membrane and dissociate the EV and cell-specific markers. The detergent treatment followed by SEC and Lumin-EX, with CD9, CD63, CD235 and GAP43 capture, respectively, followed by pan-TSPN detection (Fig. 6) showed in significant signal reduction in the early fractions, due to detergent treatment (Fig. 6A-C). The same treatment also strongly reduced the signal in late fractions, resulting from GAP43 capture and pan-TSPN detection (Fig. 6C, D). The shift following detergent treatment of CD63 and CD235 signals towards late fractions (Fig. 6C, D) may reflect the closure of residual membranes and formation of smaller vesicles. A potential cause of reduced detergent sensitivity of the smaller particles is their distinct lipid composition, e.g., higher lipid raft content (Sonnino and Prinetti 2013), which is supported by the lipid content analysis below.

Interestingly, CD63 and CD81 capture beads, in addition to large peaks in early fractions, also generated disperse positive signal in late fractions (Fig. 5E-G) T consistent with previous findings, where the analysis qEV fractions for CD63 and CD81 content yielded a continuous signal stretching towards late SEC fractions (Ter-Ovanesyan et al. 2021). While this was interpreted as contamination, similar distribution was less pronounced in EV from cell culture media (Fig. 7) and may reflect a broader EV size distribution in blood plasma.

SEC late fractions contain typical EV mRNA and lipids

It is generally assumed that the late fractions generated by size exclusion chromatography do not contain extracellular vesicles; however, Lumin-EX showed that the late fractions comprise significant levels of tetraspanins, are sensitive to detergent treatment and contain small spherical particles, a typical EV hallmarks defined by MISEV (Thery et al. 2018). To further characterize these particles, we examined RNA and lipid content of pooled fractions 1–5 and 8–15 combined and concentrated by spin-filtration (100 kDa MWCO). EV are the main carrier of cell-free mRNA (Jose 2015; O'Brien et al. 2020). Multiple cell-specific mRNAs were measured by qPCR (Tables 4A-C) using an amplicon-based approach (TaqMan primers, Table 3). An approximately 2-fold lower GAPDH content in fractions 8–15 indicates higher overall RNA levels in fractions 1–6, consistent with the larger vesicle size. However, multiple mRNA were clearly detectable in fractions 8–15 and normalization to

GAPDH, revealed up to 4-fold enrichment of neuron-specific transcripts, neurogranin (NRGN) and Orexin (HTCR), and oligodendrocyte markers SOX1 and OLIG2 (Table 4A). This is consistent with the observed high levels of neuron-specific proteins GAP43 and CD171in the late fractions. In addition, the ratios of neuron specific NRGN mRNA to erythrocytic and platelet mRNA (HBB and PF4) were significantly higher in these fractions (Tables 4A, B). Together, these findings point to distinct cellular origins of EV populations in the early and late fractions, and the predominance of neuronal markers in the smaller EV-like particles.

Table 4A
mRNA enrichment in pooled SEC fractions (normalized to GAPDH)

Gene transcript	**ΔCt**		**Late/early ratio**
	Early fractions	**Late fractions**	
NRGN	2.362234	0.407699	3.875911
SOX1	2.589385	0.71876812	3.656889
OLIG1	2.192837	1.758674622	1.351127
OLIG2	-2.35433	-3.76834	2.664775

Crude Plasma EV preparations were resolved by SEC (qEV original, 35 nm, Izon Sciences). Early (2–5) and late (9–15) fractions were pooled together and concentrated by spin filtration (100kDa MWCO). Total RNA was isolated and indicated transcripts measured by qRT-PCR with specific primers (Table 3). ΔCt values were calculated using a housekeeping gene, GAPDH, as an internal control.

Table 4B

Neuronal and erythrocytic mRNA content in pooled SEC fractions

Gene transcript	Ct		DCT (to HBB)		Ratio to HBB transcript	
	Early fractions	Late fractions	Early fractions	Late fractions	Early fractions	Late fractions
NRGN	22.99162312	23.04724693	-5.61276	-8.06409931	48.93386414	267.6306081
SOX1	28.92022133	28.06206989	0.315836906	-3.04927635	0.803384813	8.277966166
OLIG1	28.52367401	29.10197639	-0.08071041	-2.00936985	1.057538665	4.026063286
OLIG2	23.97650909	23.57496071	-4.62787532	-7.53638553	24.7246009	185.6427979
HBB	28.60438442	31.11134624	-	-		

Crude Plasma EV preparations were resolved by SEC (qEV original, 35 nm, Izon Sciences). Early (2-5) and late (9-15) fractions were pooled together and concentrated by spin filtration (100kDa MWCO). Total RNA was isolated and indicated transcripts measured by qRT-PCR with specific primers (Table 3). Ct values are shown. The enrichment for neuronal mRNA was calculated as were calculated DCt values compared to HBB, an erythrocyte marker.

Table 4C

Neuronal and platelet mRNA content in pooled SEC fractions

Gene transcript	Ct		DCT (to HBB)		Ratio to PF4 transcript	
	Early fractions	Late fractions	Early fractions	Late fractions	Early fractions	Late fractions
NRGN	22.99162312	23.04724693	-9.07498531	-13.4121246	539.3153602	10900.63556
SOX1	28.92022133	28.06206989	-3.1463871	-8.39730167	8.854354284	337.1628269
OLIG1	28.52367401	29.10197639	-3.54293441	-7.35739517	11.65546306	163.9821729
OLIG2	23.97650909	23.57496071	-8.09009933	-12.8844108	272.4975285	7561.259528
PF4	32.06660843	36.45937157	-	-	-	-

Crude Plasma EV preparations were resolved by SEC (qEV original, 35 nm, Izon Sciences). Early (2-5) and late (9-15) fractions were pooled together and concentrated by spin filtration (100kDa MWCO). Total RNA was isolated and indicated transcripts measured by qRT-PCR with specific primers (Table 3). Ct values are shown. The enrichment for neuronal mRNA was calculated as were calculated DCt values compared to PF4, a platelet marker.

Pooled fractions 1–5 and 8–15 were subjected to lipidomic analysis by Ultra Performance Liquid Chromatography-Tandem Mass Spectrometry (UPLC-MSMS). The lipid content of fractions 8–15 was consistent with the published lipidomic analyses of EV membranes (Yanez-Mo et al. 2015; Skotland et al. 2020). For the major lipid classes (cholesterol, phosphatidylcholine and PC ethers, phosphatidylserine, phosphatidyl-ethanolamine and PE ethers, diglycerides, phosphoglycerates, phosphatidic acid, phosphatidylinositol, ceramide and lactoceramide), the measured percentage of total lipid content in the late and early EV fractions, remained within the previously observed range. However, there were differences in lipid composition of the early (1–6) and late (8–15) fractions (Table 5 and Fig. 8). Free cholesterol was lower in the late fractions, likely due to sequestration in protein complexes involved in cholesterol transport (Cockcroft 2021; Zanotti et al. 2021). In agreement, phosphatidylethanolamine (PE), PE esters, phosphatidylcholine, and phosphatidylserine were 2–3 times higher in fractions 8–15 compared to the early fractions (Table 5). Further, a significant 2.5-fold increase in sphingomyelin (SM) and increased SM/cholesterol ratio in late fractions are likely due to increased proportion of lipid rafts (Simons and Ehehalt 2002; Ouweneel et al. 2020; Shaw et al. 2021). Given slightly lower sensitivity of these fractions to detergent treatment, our observations suggest higher lipid raft content in smaller EV, compared to canonical EV eluted in early fractions. Together, these findings strengthen our interpretation wherein the signal detected by Lumin-EX in the late SEC fractions represents EV subpopulations rather than protein contamination.

Table 5
Lipid content of the late and early pooled SEC fractions

Lipid species	% Total lipid				Late/ Early ratio	P value (T-test)
	Early fractions		Late fractions			
	Average	Std	Average	Std		
Cholesterol	58.84417	12.78809	31.17807	1.001808	0.524965	0.013858
Phosphatidylethanolamine	7.185072	1.791263	18.09836	2.149141	2.518883	0.006269
Phosphatidylethanolamine esters	6.556616	1.639689	16.15601	1.432092	2.464078	0.010448
Phosphatidylcholine	5.06497	3.500439	16.9832	1.808727	3.35308	0.001742
Phosphatidylserine	2.803951	0.032804	5.460818	0.094241	1.947544	3.71E-05
Dihydrosphingomyelin	2.661473	0.419849	0.561044	0.017827	0.210802	0.04453
Sphingomyelin	2.066918	0.116012	5.86615	0.229976	2.838114	0.000206
Sulfatide	1.044329	0.121476	0.423145	0.051607	0.405184	0.030678
Ceramide	1.015121	0.101341	0.590466	0.026987	0.58167	0.046919
Phosphatidylinositol	1.009969	0.116646	2.007596	0.204886	1.987779	0.003097
Lactosyl-ceramide	0.804356	0.202362	0.153533	0.017996	0.190877	0.068087
Phospho-ceramide	0.344956	0.030619	1.191594	0.100097	3.454337	0.001015
Monohexosyl-ceramide	0.33583	0.01688	0.285899	0.019925	0.851319	0.034268
Lyso-phosphatidyl ethanolamine	0.222608	0.028278	0.142429	0.020116	0.63982	0.046703
Monoglycerides	0.177055	0.004027	0.640425	0.240593	3.617098	0.039629
Cholesterol esters	0.17601	0.009814	0.263788	0.045196	1.498709	0.035008
Lyso-phosphatidyl choline	0.15395	0.015923	0.087663	0.007112	0.569427	0.038256
Lyso-phosphatidylethanolamine	0.145211	0.020561	0.068489	0.011437	0.471648	0.03779
Diglycerides	0.1258	0.045601	0.058413	0.009868	0.464329	0.138111

Crude Plasma EV preparations were resolved by SEC (qEV original, 35 nm, Izon Sciences). Early (2–5) and late (9–15) fractions were pooled together and concentrated by spin filtration (100kDa MWCO). Total RNA was isolated and indicated lipids measured as described in Methods. For each individual lipid, the percentage of total lipid content was calculated. Four individual preparations were compared, and P values are shown.

Cultured human neurons release larger EV

To compare size distribution of EV found in blood plasma and released by the cultured cells, we examined EV from iPSC-derived cortical neurons (BrainXell). Conditioned medium concentrated by ultrafiltration was subjected

to SEC (qEV Original, IZON Sciences), and the fractions analyzed by Lumin-EX with capture beads for GAP43, CD171 and CD235 and pan-TSPN detection cocktail (Fig. 7A-C). Consistent with their neuronal origin, EV found in early fractions showed strong positivity for GAP43 and CD171 (Fig. 7A, B); however, ~ 10% of the GAP43 and CD171 signal was found the late fractions. Consistent with the neuronal phenotype, Lumin-EX with CD235 beads yielded no detectable signal (Fig. 8C).

In addition, the same qEV fractions were analyzed using CD9, CD63 and CD81 beads followed by GAP43 detection (Fig. 8D-F). All tetraspanins eluted with a similar pattern, a peak in the early fractions and disperse signal in late fractions, suggesting that cultured cells predominantly release larger EV. The CD63 and CD81 signals in the EV from iPSC-derived neurons were by an order of magnitude higher than CD9 signal, suggesting that while EV size distribution in neuronal cell culture is different from plasma, their TSPN composition remains similar, with relative paucity of CD9.

Discussion

Our goal was a reliable, user-friendly assay for a rapid multifactorial EV profiling in biofluids. EV released from most tissues/organs are found in a variety of bodily fluids. Since EV offer molecular snapshots of the cells of origin, their promise as an emerging diagnostic platform is hard to overestimate (Simpson et al. 2009; He et al. 2018; Hunter and Dhaun 2020; Alberro et al. 2021; Heydari et al. 2021; Liu et al. 2021; Thakur et al. 2021; Trino et al. 2021). However, EV isolation and characterization are hindered by their extreme heterogeneity that extends to EV size, composition, and surface antigen profiles and limits EV implementation in clinical practice (Quiroz-Baez et al. 2020; Bordanaba-Florit et al. 2021; Claridge et al. 2021; Cloet et al. 2021; Singh et al. 2021).

Characterization of EV surface proteins, an integral part of MISEV guidelines, is a valuable approach, in aid of defining diverse subpopulations in complex EV pools found in biofluids. Here, we describe the development of a straightforward and robust technique for simultaneous, multiplexed detection and assessment of EV surface proteins. This novel method, based on a sandwich principle, is applied to intact EV, with two antibodies against distinct proteins presumably connected by the EV membrane. This concept has been exploited for EV analysis, in assays ranging from ELISA to microfluidic devices. Here we pair this approach with the Luminex platform, which strategically combines high sensitivity with the ease of multiplexing. Importantly, our method, Lumin-EX, is optimized for the use with unprocessed plasma, thus bypassing lengthy and cumbersome steps of EV isolation, enrichment, and purification.

Assay validation according to the published guidelines for EV flow cytometry and FDA guidelines for immunoassay development requires linear signal in proportion to the antibody and antigen input concentration. Lumin-EX yielded linearity across 16-fold antibody and plasma dilutions, with antibody concentration between 0.07-2.0 ug/ml ($R = 0.9$) and 8–33-fold plasma dilution, an acceptable linearity range. However, due to the variance introduced by multiple antibodies and plasma specimens, relatively narrow ranges observed for some antibody and plasma suggest further optimization of working dilutions for at least some analytes

The specificity requirements for the EV analysis platform are twofold: the selectivity for EV and specificity for the chosen antigen (surface EV protein). Lumin-EX selectivity toward EV was demonstrated using two methods for EV depletion, PEG precipitation and EV lysis. In both cases there was a significant (over 50%) reduction in the measured signal. Antibody specificity was assessed using comparison with non-specific, isotype-matched

control antibodies (IgG) and by using sandwich combinations of the antibodies targeting surface markers of distinct cell types, for divergent EV subpopulations, e.g., erythrocytic, neuronal or macrophage-derived. For example, capture with Lumin-EX beads against CD235 (erythrocyte marker) yielded clear signal upon detection with a tetraspanin antibody cocktail (a combination of common EV markers), but not with the antibodies against neuronal markers CD171 and GAP43 or a macrophage marker, CD68. This confirms Lumin-EX specificity for both EV and chosen analytes, in this case population-specific surface proteins. Moreover, the data ascertain Lumin-EX utility to assess co-localization of EV surface proteins, a feature that can be exploited for the analysis and characterization of EV subtypes in blood plasma and in cell culture media.

Moreover, EV released by genetically manipulated HEK cells, expressing a single neuronal antigen, either CD171 or GAP43, were captured only using beads decorated with the appropriate antibody. No cross-reactivity with another neuronal marker, or erythrocyte marker was observed. Similarly, EV from iPSC-derived neurons yielded detectable signal if captured with the beads targeting neuronal (CD171, GAP43) and EV antigens (CD63, CD81), but not with CD235 beads. The presence of CD171 on neuronal EV generated in cell culture is in keeping with previous reports (Faure et al. 2006; Lachenal et al. 2011; Shi et al. 2014; Norman et al. 2021) and detection of GAP43/neuromodulin (Pfenninger et al. 1991), another neuron-specific membrane protein, further corroborates Lumin-EX specificity. Together, our results clearly support assay specificity.

Following Lumin-EX qualification with a single capture bead, we demonstrated its multiplexing capacity, particularly important for generation of complex datasets from the low-abundance samples collected in clinical studies. Single and multiplexed assays showed similar linearity and detection ranges for at least six EV markers, in an assay that combines up to 6 analytes. Moreover, the analysis of tetraspanin levels in plasma EV from 20 donors showed considerable variability between individuals, and strong (R^2 = 0.93) correlation between the values generated using single and multiplexed Lumin-EX. In the future, such multiplexed assay may be employed for population-wide studies of tissue-specific EV species in blood plasma (EV profiling).

For additional EV attribution of the Lumin-EX signal, the assay was coupled with a standard EV isolation procedure, size SEC on pre-calibrated columns (Monguio-Tortajada et al. 2019; Kurian et al. 2021; Stam et al. 2021). Interestingly, while some tissue-specific (CD235) and all EV-specific probes generated clear signal in early fractions (1–5) expected to contain the majority of EVs, capture beads for tetraspanins CD63 and CD81, as well as for cell markers CD171, GAP43 and CD68, yielded distinctive signals in late fractions (8–17). The localization of CD171, and the trailing of CD63 and CD81 signal to the late SEC fractions was documented previously (Norman et al. 2021; Ter-Ovanesyan et al. 2021); however, it was attributed to overabundance of soluble protein. Conversely, such signal could be generated by a smaller EV subpopulation. Using Lumin-EX with tetraspanins for capture and cell-specific antigens for detection, and vice versa, we observed strong signals in the late SEC fractions. The EV origin of the signal was supported by the detection and capture with tetraspanin antibodies. Transmission electron microscopy of the late fractions also shows spherical objects 10–30 nm in diameter consistent with vesicular structures. Furthermore, late fractions contain lipids and mRNA characteristic of EV. Critically, detergent pre-treatment prior to analysis dramatically reduced Lumin-EX signal, both in the early and late fractions. Altogether, our experiments point to the presence of smaller EV in the late SEC fractions, detectable by Lumin-EX. Interestingly, similar analysis of the media conditioned by iPSC derived neurons revealed both GAP43 and CD171 signals predominantly in the early fractions, and a much weaker signal in the late fractions, suggesting that smaller EV are enriched in plasma compared to the culture media. This could be explained by the advantage smaller vesicles have entering circulation, or smaller EV generation by extrusion via the vascular wall.

The notion that many tissue-derived EV in the plasma are eluted in the late fractions is supported by the detection in these fractions of EV surface markers specific for neurons, tissue macrophages and podocytes, while the markers of circulating cells, e.g., erythrocytes, are found in earlier fractions. Moreover, qPCR showed a much higher ratio of neuronal and oligodendrocyte-specific transcripts, to erythrocyte-specific mRNA in the late fractions, compared to the early ones. Importantly, TaqMan PCR is amplicon-based and thus further research is needed to determine the presence of full-length and functional mRNA. Further research is needed to reveal the role and biogenesis of the putative novel EV subpopulation discovered by the innovative Lumin-EX developed herein. Our results agree with other studies, which demonstrate broader EV heterogeneity than previously postulated. For example, smaller (30–50 nm) EV with low phosphatidylserine content are enriched in blood plasma due to avoidance of capture by the blood monocytes/macrophages (Matsumoto et al. 2021) and strong positivity for EV tetraspanins and particle presence were noted in late SEC fractions (Ter-Ovanesyan et al. 2021) even though it was not attributed to EV heterogeneity. Conversely, functional small particles with diameters below 50 nm, e.g., exomeres and supermeres, have been discovered and their ability to carry functional proteins and nucleic acids documented (Zhang et al. 2018; Zhang and Lyden 2019; Zhang et al. 2019; Zhang et al. 2021). The nature, biogenesis and the manner of circulation entry of these smaller particles is subject to further studies; however, our results point to an intriguing possibility that EV in biofluids, which are subject to long-range transfer between distant organs, are distinct from EV generated by cultured cells.

Current EV research emphasizes heterogeneity of the canonical EV markers, e.g., tetraspanins, in EV populations released by divergent cell and tissue types and Lumin-EX is a useful new tool to harness such heterogeneity. For example, we show that neuronal EV both in plasma and in cell culture comprise high levels of CD63 and CD81 but not of CD9, while in erythrocytic EV CD9 content is high and CD63 and CD81 are low. In contrast, all three tetraspanins are similarly represented in EV from HEK cells. These results demonstrate a useful capability of the new Lumin-EX assay for comparative analysis of surface antigens in cell- and tissue-specific EV populations (profiling).

In conclusion, Lumin-EX, is a novel, sensitive, specific, and user-friendly assay for the analysis of EV surface proteins in culture media and especially in biological fluids. It has the advantage of multiplexing, low sample volume requirements and applicability for unprocessed plasma samples. This novel technology enabled the discovery of a smaller subpopulation of tissue specific EVs in blood plasma, which eluted in late SEC fractions, and identified differences in tetraspanin profiles between plasma EV subpopulations. This promising novel technique could be used to study EV surface protein composition and co-localization. We believe that it can inform EV subpopulation analysis in cell culture and in biological fluids and provide link between specific EV populations and their biological functions. With the interest in therapeutic EV applications growing, such assay may be also applied to control quality and consistency of EV therapeutics.

Declarations

Acknowledgements:

TEM samples were prepared and imaged by the Brandeis Electron Microscopy Facility

The study was supported in part by the Intramural Research Program of the National Institute on Aging, NIH (for E. Eren and D. Kapogiannis)

Conflict of Interest Statement:

Olga Volpert, Erez Eitan and Katia Elgart are currently employed by NeuroDex Inc., a for-profit start-up company focused on EV-based diagnostic assay development and commercialization, EG was an employee of NeuroDex at the time the work was conducted. EE is also a majority shareholder at NeuroDex. All other authors have no competing interests

Data availability Statement:

All primary data is available upon request. Please contact a corresponding author, Olga V Volpert (ovolpert@neurodex.co)

Ethics approval statement:

All human plasma and serum samples were obtained from a commercial source (BioIVT), where the accepted standards for sample collection and storage are ensured by internal ethics committee.

References

1. Alberro A, Iparraguirre L, Fernandes A, Otaegui D. 2021. Extracellular Vesicles in Blood: Sources, Effects, and Applications. Int J Mol Sci **22**.
2. Bligh EG, Dyer WJ. 1959. A rapid method of total lipid extraction and purification. Can J Biochem Physiol **37**: 911–917.
3. Bordanaba-Florit G, Royo F, Kruglik SG, Falcon-Perez JM. 2021. Using single-vesicle technologies to unravel the heterogeneity of extracellular vesicles. Nat Protoc **16**: 3163–3185.
4. Chan RB, Oliveira TG, Cortes EP, Honig LS, Duff KE, Small SA, Wenk MR, Shui G, Di Paolo G. 2012. Comparative lipidomic analysis of mouse and human brain with Alzheimer disease. J Biol Chem **287**: 2678–2688.
5. Chiang CY, Chen C. 2019. Toward characterizing extracellular vesicles at a single-particle level. J Biomed Sci **26**: 9.
6. Claridge B, Lozano J, Poh QH, Greening DW. 2021. Development of Extracellular Vesicle Therapeutics: Challenges, Considerations, and Opportunities. Front Cell Dev Biol **9**: 734720.
7. Cloet T, Momenbeitollahi N, Li H. 2021. Recent advances on protein-based quantification of extracellular vesicles. Anal Biochem **622**: 114168.
8. Cockcroft S. 2021. Mammalian lipids: structure, synthesis and function. *Essays Biochem*.
9. Colombo M, Raposo G, Thery C. 2014. Biogenesis, secretion, and intercellular interactions of exosomes and other extracellular vesicles. Annu Rev Cell Dev Biol **30**: 255–289.
10. Faure J, Lachenal G, Court M, Hirrlinger J, Chatellard-Causse C, Blot B, Grange J, Schoehn G, Goldberg Y, Boyer V et al. 2006. Exosomes are released by cultured cortical neurones. Molecular and cellular neurosciences **31**: 642–648.
11. Graham H, Chandler DJ, Dunbar SA. 2019. The genesis and evolution of bead-based multiplexing. Methods **158**: 2–11.

12. Guan Z, Li S, Smith DC, Shaw WA, Raetz CR. 2007. Identification of N-acylphosphatidylserine molecules in eukaryotic cells. Biochemistry **46**: 14500–14513.
13. He C, Zheng S, Luo Y, Wang B. 2018. Exosome Theranostics: Biology and Translational Medicine. Theranostics **8**: 237–255.
14. He J, Liu G, Dou S, Gupta S, Rusckowski M, Hnatowich D. 2007. An improved method for covalently conjugating morpholino oligomers to antitumor antibodies. Bioconjug Chem **18**: 983–988.
15. Heydari R, Abdollahpour-Alitappeh M, Shekari F, Meyfour A. 2021. Emerging Role of Extracellular Vesicles in Biomarking the Gastrointestinal Diseases. Expert Rev Mol Diagn **21**: 939–962.
16. Hsu FF, Turk J, Shi Y, Groisman EA. 2004. Characterization of acylphosphatidylglycerols from Salmonella typhimurium by tandem mass spectrometry with electrospray ionization. J Am Soc Mass Spectrom **15**: 1–11.
17. Hunter RW, Dhaun N. 2020. Extracellular RNA in kidney disease: moving slowly but surely from bench to bedside. Clin Sci (Lond) **134**: 2893–2895.
18. Jose AM. 2015. Movement of regulatory RNA between animal cells. Genesis **53**: 395–416.
19. Kanwar SS, Dunlay CJ, Simeone DM, Nagrath S. 2014. Microfluidic device (ExoChip) for on-chip isolation, quantification and characterization of circulating exosomes. Lab Chip **14**: 1891–1900.
20. Kosanovic M, Milutinovic B, Goc S, Mitic N, Jankovic M. 2017. Ion-exchange chromatography purification of extracellular vesicles. Biotechniques **63**: 65–71.
21. Kurian TK, Banik S, Gopal D, Chakrabarti S, Mazumder N. 2021. Elucidating Methods for Isolation and Quantification of Exosomes: A Review. Mol Biotechnol **63**: 249–266.
22. Lachenal G, Pernet-Gallay K, Chivet M, Hemming FJ, Belly A, Bodon G, Blot B, Haase G, Goldberg Y, Sadoul R. 2011. Release of exosomes from differentiated neurons and its regulation by synaptic glutamatergic activity. Molecular and cellular neurosciences **46**: 409–418.
23. Liu Q, Piao H, Wang Y, Zheng D, Wang W. 2021. Circulating exosomes in cardiovascular disease: Novel carriers of biological information. Biomed Pharmacother **135**: 111148.
24. Matsumoto A, Takahashi Y, Ogata K, Kitamura S, Nakagawa N, Yamamoto A, Ishihama Y, Takakura Y. 2021. Phosphatidylserine-deficient small extracellular vesicle is a major somatic cell-derived sEV subpopulation in blood. iScience **24**: 102839.
25. Monguio-Tortajada M, Galvez-Monton C, Bayes-Genis A, Roura S, Borras FE. 2019. Extracellular vesicle isolation methods: rising impact of size-exclusion chromatography. Cell Mol Life Sci **76**: 2369–2382.
26. Nolan JP, Duggan E. 2018. Analysis of Individual Extracellular Vesicles by Flow Cytometry. Methods Mol Biol **1678**: 79–92.
27. Norman M, Ter-Ovanesyan D, Trieu W, Lazarovits R, Kowal EJK, Lee JH, Chen-Plotkin AS, Regev A, Church GM, Walt DR. 2021. L1CAM is not associated with extracellular vesicles in human cerebrospinal fluid or plasma. Nat Methods **18**: 631–634.
28. O'Brien K, Breyne K, Ughetto S, Laurent LC, Breakefield XO. 2020. RNA delivery by extracellular vesicles in mammalian cells and its applications. Nat Rev Mol Cell Biol **21**: 585–606.
29. Ohmichi T, Mitsuhashi M, Tatebe H, Kasai T, Ali El-Agnaf OM, Tokuda T. 2019. Quantification of brain-derived extracellular vesicles in plasma as a biomarker to diagnose Parkinson's and related diseases. Parkinsonism Relat Disord **61**: 82–87.

30. Ouweneel AB, Thomas MJ, Sorci-Thomas MG. 2020. The ins and outs of lipid rafts: functions in intracellular cholesterol homeostasis, microparticles, and cell membranes: Thematic Review Series: Biology of Lipid Rafts. J Lipid Res **61**: 676–686.
31. Pfenninger KH, de la Houssaye BA, Helmke SM, Quiroga S. 1991. Growth-regulated proteins and neuronal plasticity. A commentary. Mol Neurobiol **5**: 143–151.
32. Quiroz-Baez R, Hernandez-Ortega K, Martinez-Martinez E. 2020. Insights Into the Proteomic Profiling of Extracellular Vesicles for the Identification of Early Biomarkers of Neurodegeneration. Front Neurol **11**: 580030.
33. Rak J. 2010. Microparticles in cancer. Semin Thromb Hemost **36**: 888–906.
34. Shaw TR, Ghosh S, Veatch SL. 2021. Critical Phenomena in Plasma Membrane Organization and Function. Annu Rev Phys Chem **72**: 51–72.
35. Shi M, Liu C, Cook TJ, Bullock KM, Zhao Y, Ginghina C, Li Y, Aro P, Dator R, He C et al. 2014. Plasma exosomal alpha-synuclein is likely CNS-derived and increased in Parkinson's disease. Acta neuropathologica **128**: 639–650.
36. Simons K, Ehehalt R. 2002. Cholesterol, lipid rafts, and disease. J Clin Invest **110**: 597–603.
37. Simpson RJ, Lim JW, Moritz RL, Mathivanan S. 2009. Exosomes: proteomic insights and diagnostic potential. Expert Rev Proteomics **6**: 267–283.
38. Singh K, Nalabotala R, Koo KM, Bose S, Nayak R, Shiddiky MJA. 2021. Separation of distinct exosome subpopulations: isolation and characterization approaches and their associated challenges. Analyst **146**: 3731–3749.
39. Skotland T, Sagini K, Sandvig K, Llorente A. 2020. An emerging focus on lipids in extracellular vesicles. Adv Drug Deliv Rev **159**: 308–321.
40. Sonnino S, Prinetti A. 2013. Membrane domains and the "lipid raft" concept. Curr Med Chem **20**: 4–21.
41. Stam J, Bartel S, Bischoff R, Wolters JC. 2021. Isolation of extracellular vesicles with combined enrichment methods. J Chromatogr B Analyt Technol Biomed Life Sci **1169**: 122604.
42. Ter-Ovanesyan D, Norman M, Lazarovits R, Trieu W, Lee JH, Church GM, Walt DR. 2021. Framework for rapid comparison of extracellular vesicle isolation methods. Elife **10**.
43. Thakur A, Ke X, Chen YW, Motallebnejad P, Zhang K, Lian Q, Chen HJ. 2021. The mini player with diverse functions: extracellular vesicles in cell biology, disease, and therapeutics. *Protein Cell*.
44. Thery C Witwer KW Aikawa E Alcaraz MJ Anderson JD Andriantsitohaina R Antoniou A Arab T Archer F Atkin-Smith GK et al. 2018. Minimal information for studies of extracellular vesicles 2018 (MISEV2018): a position statement of the International Society for Extracellular Vesicles and update of the MISEV2014 guidelines. Journal of extracellular vesicles **7**: 1535750.
45. Trino S, Lamorte D, Caivano A, De Luca L, Sgambato A, Laurenzana I. 2021. Clinical relevance of extracellular vesicles in hematological neoplasms: from liquid biopsy to cell biopsy. Leukemia **35**: 661–678.
46. Welsh JA, Van Der Pol E, Arkesteijn GJA, Bremer M, Brisson A, Coumans F, Dignat-George F, Duggan E, Ghiran I, Giebel B et al. 2020. MIFlowCyt-EV: a framework for standardized reporting of extracellular vesicle flow cytometry experiments. J Extracell Vesicles **9**: 1713526.
47. Witwer KW, Thery C. 2019. Extracellular vesicles or exosomes? On primacy, precision, and popularity influencing a choice of nomenclature. J Extracell Vesicles **8**: 1648167.

48. Yanez-Mo M, Siljander PR, Andreu Z, Zavec AB, Borras FE, Buzas EI, Buzas K, Casal E, Cappello F, Carvalho J et al. 2015. Biological properties of extracellular vesicles and their physiological functions. Journal of extracellular vesicles **4**: 27066.

49. Zanotti I, Poti F, Cuchel M. 2021. Hdl and Reverse Cholesterol Transport in Humans and Animals: Lessons from Pre-Clinical Models and Clinical Studies. Biochim Biophys Acta Mol Cell Biol Lipids: 159065.

50. Zhang H, Freitas D, Kim HS, Fabijanic K, Li Z, Chen H, Mark MT, Molina H, Martin AB, Bojmar L et al. 2018. Identification of distinct nanoparticles and subsets of extracellular vesicles by asymmetric flow field-flow fractionation. Nat Cell Biol **20**: 332–343.

51. Zhang H, Lyden D. 2019. Asymmetric-flow field-flow fractionation technology for exomere and small extracellular vesicle separation and characterization. Nat Protoc **14**: 1027–1053.

52. Zhang Q, Higginbotham JN, Jeppesen DK, Yang YP, Li W, McKinley ET, Graves-Deal R, Ping J, Britain CM, Dorsett KA et al. 2019. Transfer of Functional Cargo in Exomeres. Cell Rep **27**: 940–954 e946.

53. Zhang Q, Jeppesen DK, Higginbotham JN, Graves-Deal R, Trinh VQ, Ramirez MA, Sohn Y, Neininger AC, Taneja N, McKinley ET et al. 2021. Supermeres are functional extracellular nanoparticles replete with disease biomarkers and therapeutic targets. Nat Cell Biol **23**: 1240–1254.

Figures

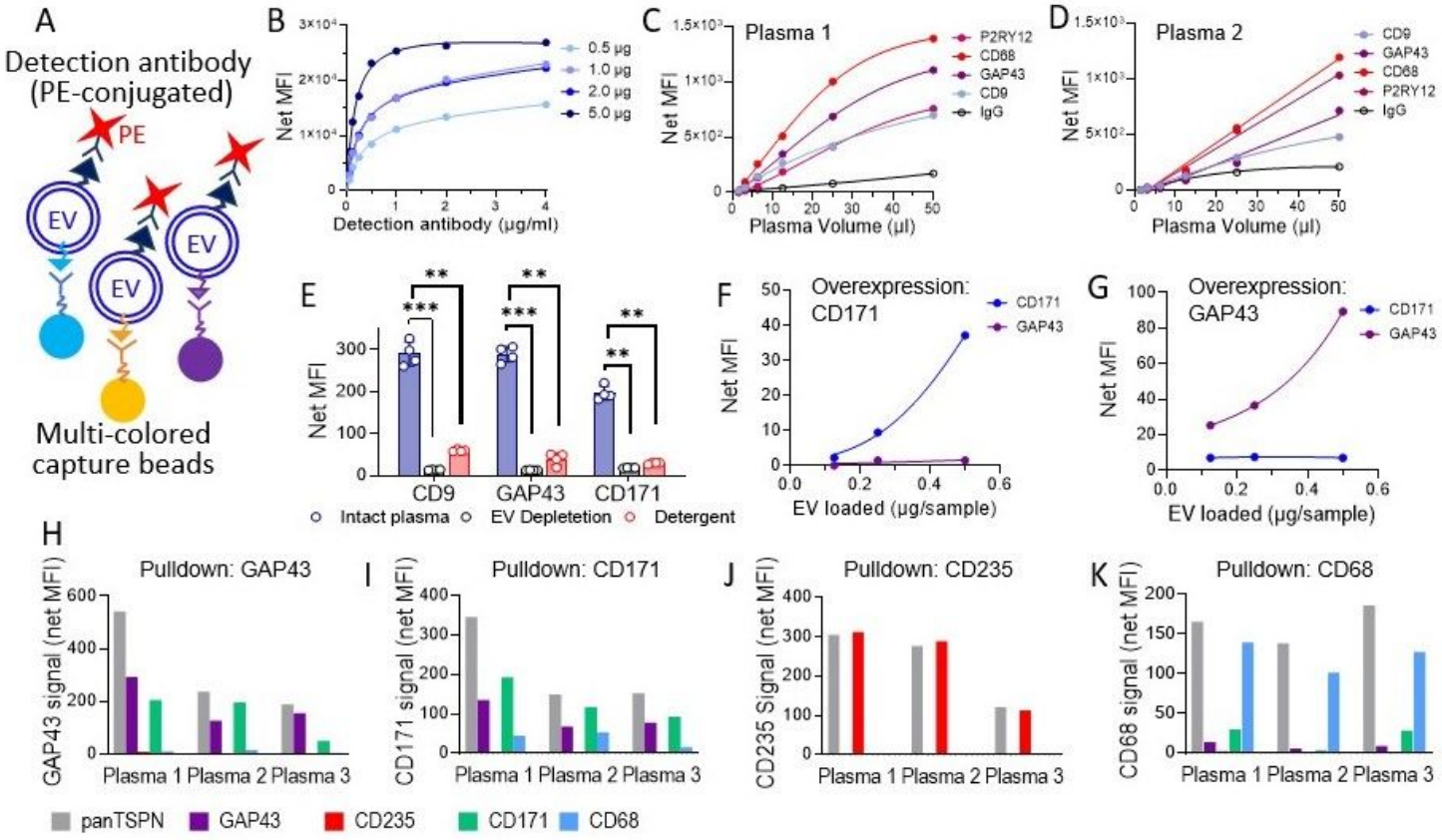

Volpert et al., Figure 1.

Figure 1

Optimization and testing of the beads for direct Luminex assessment of surface EV markers from blood plasma. **(A)** Schematic representation of Lumin-EX, a multiplexed bead-based sandwich assay. Capture beads labeled with distinct fluorophores (see Methods) are decorated with antibodies against specific surface antigens (color-coded in the diagram) and incubated with plasma or other EV-rich fluids. PE-tagged detection antibodies can vary, depending on the assay goals. Typically, a cocktail of EV markers, such as CD9, CD63 and CD81 is used. Note that capture and detection antigen should be co-localized on the surface of the same particle (connected by a plasma membrane). **(B)** Antibody loading optimization for Lumin-EX assay. MagPlex spheres are functionalized using increasing concentrations of mouse monoclonal antibodies against human CD9 (BioLegend, cat. no. 312102) in the indicated concentration range (0.5 – 5.0 mg/ml). Antibody loading was assessed by incubation of beads with increasing concentrations of PE-conjugated goat anti-mouse antibodies (BioLegend cat. No. 405307) and the signal measured in a Luminex200 plate reader following standard procedure. **(C, D)** Quantitative detection of specific EV populations in two distinct plasma samples. MagPlex beads loaded with the indicated primary antibody (1 mg/ml) and 250 beads/sample were used to probe unprocessed human plasma (BioIVT). Plasma samples were diluted as indicated in 1x PBS supplemented with 1%BSA (see Methods). Beads loaded with non-specific mouse IgG were used as a negative control. The detection was conducted using the cocktail of biotinylated pan-TSPN specific antibodies followed by incubation with SAPE reagent (see methods). Note a dose-dependent signal with a clear linear range and sample-specific differences attributable to unique representation of specific EV populations. **(E)** Plasma samples were depleted of EV prior to analysis, by polymer precipitation, or by detergent lysis (see Methods). All samples were probed with CD9-conjugated MagPlex spheres (capture beads) and the signal detected with pan-TSPN antibody cocktail. Note significantly lower signal following EV depletion or detergent lysis (**, $P<0.001$; ***, $P<0.0001$ by Tukey's multiple comparison's test). **(F, G)** EV were isolated by ion exchange chromatography from cell culture media conditioned by HEK293 cells overexpressing neuron-specific antigens CD171 (F) and GAP43 (G). The EV were diluted in 1xPBS supplemented with 1% BSA and the samples probed with the beads conjugated with antibodies against human CD171 and GAP43, respectively, followed by pan-TSPN antibody cocktail for detection. Note the lack of non-specific detection. **(H-K)** Plasma samples were analyzed using GAP43 (H), CD171 (I), CD235 (J) and CD68 (K) Lumin-EX capture beads paired with the indicated detection antibodies (pan-TSPN cocktail, GAP43, CD171, CD68 and CD235).

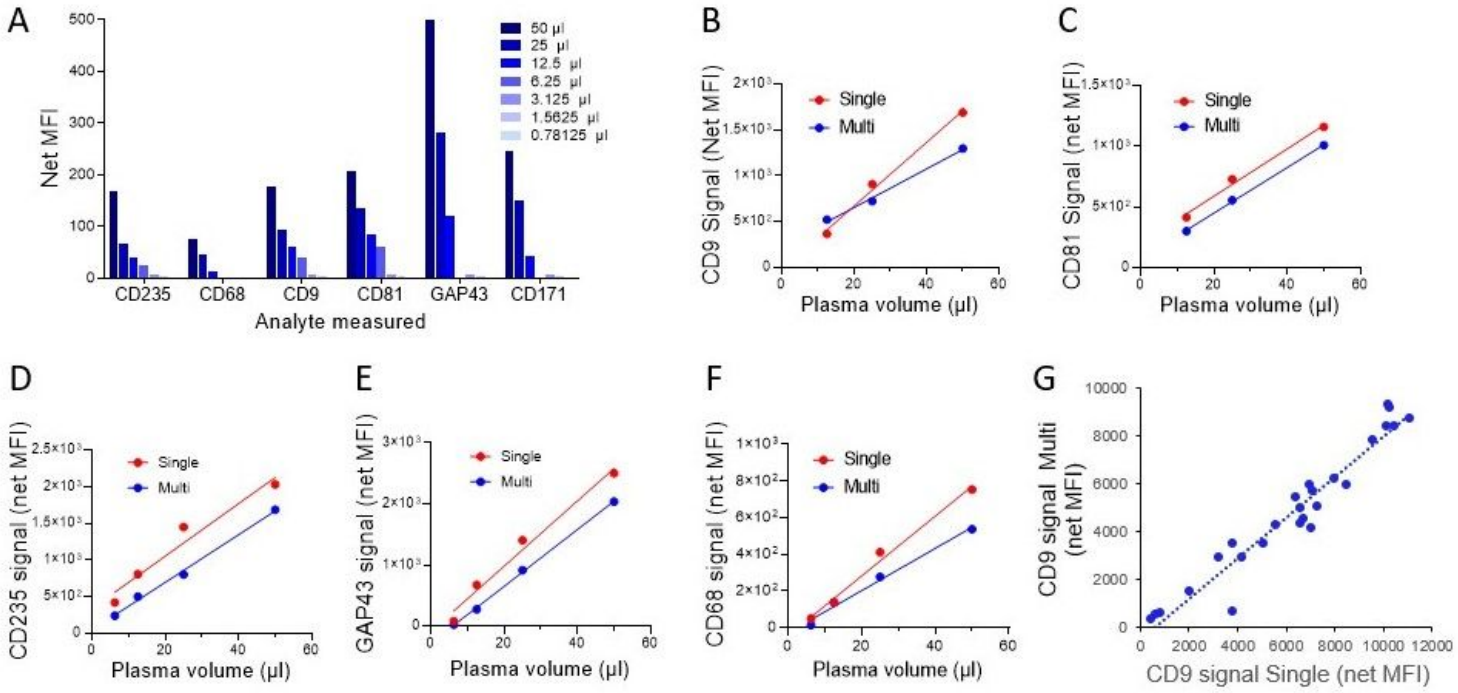

Figure 2

Lumin-EX allows simultaneous measurement of at least six surface EV proteins. (A) A multiplexed assay for simultaneous detection of EV populations expressing major tetraspanins, CD9, CD63 and CD81, together with the two neuron-specific markers (CD171 and GAP43) was used to examine the indicated dilutions of unprocessed human plasma. Note a linear range signal detected in 1-50 ml range of blood volumes. **(B-G)** Unprocessed plasma samples were subjected to Lumin-EX with indicated antibodies in a multiplexed (M) and single-bead (S) format and the values for each antibody plotted together for pairwise comparison. Note close absolute values and linearity in a similar dilution range (10-50 ml plasma per reaction). **(H)** Twenty-five postmortem plasma samples were subjected to Lumin-EX in a multiplex and a single-bead format (25 ml/sample) and the values for CD9 compared. Note strong correlation between individual values determined by multiplexed and signgle-plexed measurements.

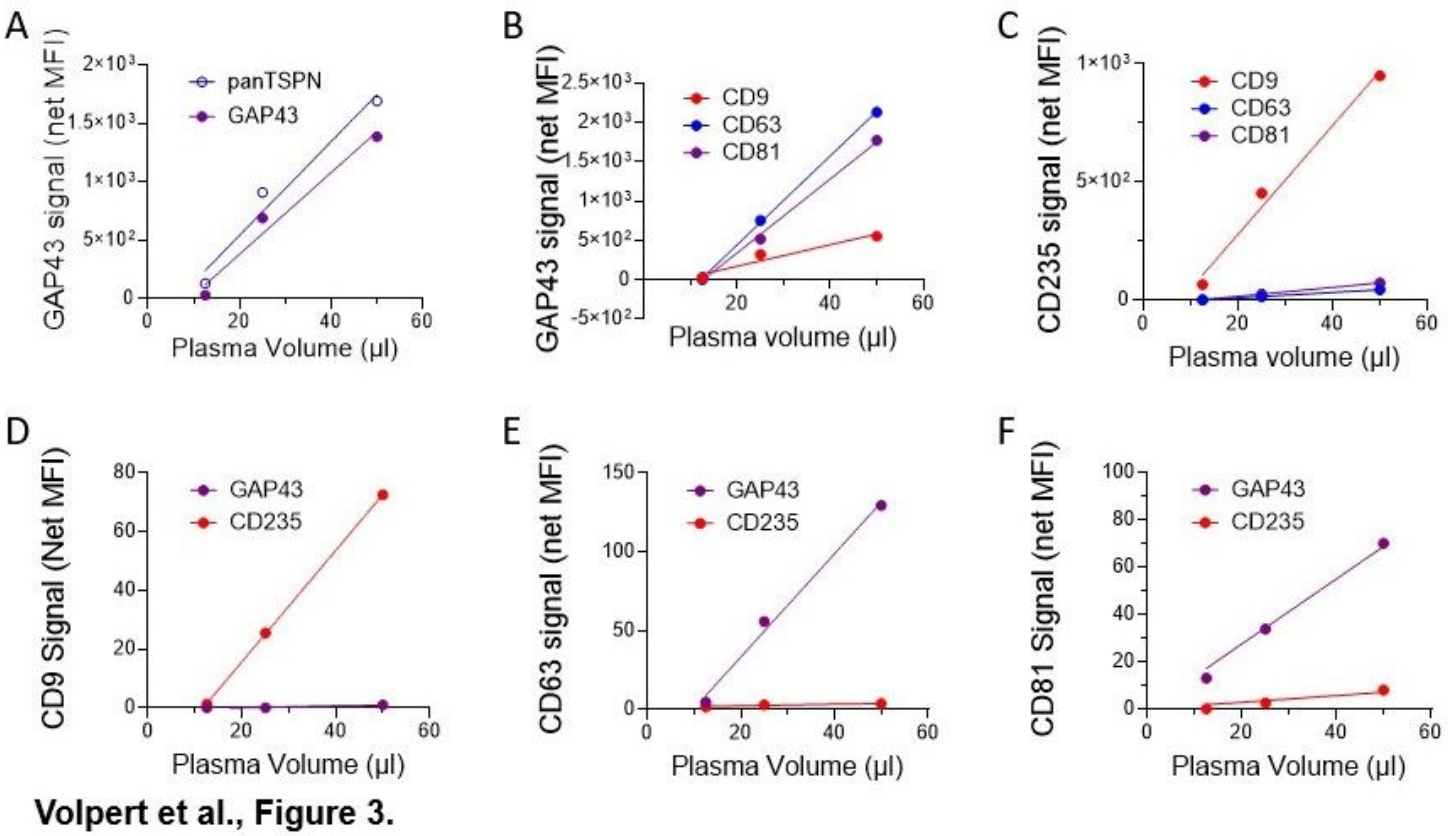

Figure 3

Lumin-EX reveals cell type specific differences in the tetraspanin profiles of distinct EV populations in blood plasma. (A) Whole plasma (10-50 ml/sample) was subjected to Lumin-EX with antibodies against axonal marker, GAP43 followed by detection with GAP43 antibodies or with pan-TSPN antibody cocktail. Similar values obtained for each detection method suggest that GAP43 in blood plasma is predominantly EV-associated. **(B)** Lumin-EX was performed using GAP43 capture beads and detection with individual tetraspanins, CD9, CD63 and CD81. Note lower CD9 levels on GAP43-positive EV. **(C)** Lumin-EX of erythrocytic EVs using capture beads for CD235/glycophorin A, followed by detection with antibodies for individual tetraspanins, CD9, CD63 and CD81. Note the high level of CD9 expression and negligible levels of CD63 and CD81. **(D)** Lumin-EX with capture beads for CD9, an EV marker, followed by detection with CD235 and GAP43 antibodies. Note low GAP43 levels and strong positivity for CD235. **(E, F)** CD63 (E), CD81 capture (F) followed by GAP43 and CD235 detection showed strong positivity for GAP43 and the lack of detectable association with CD235.

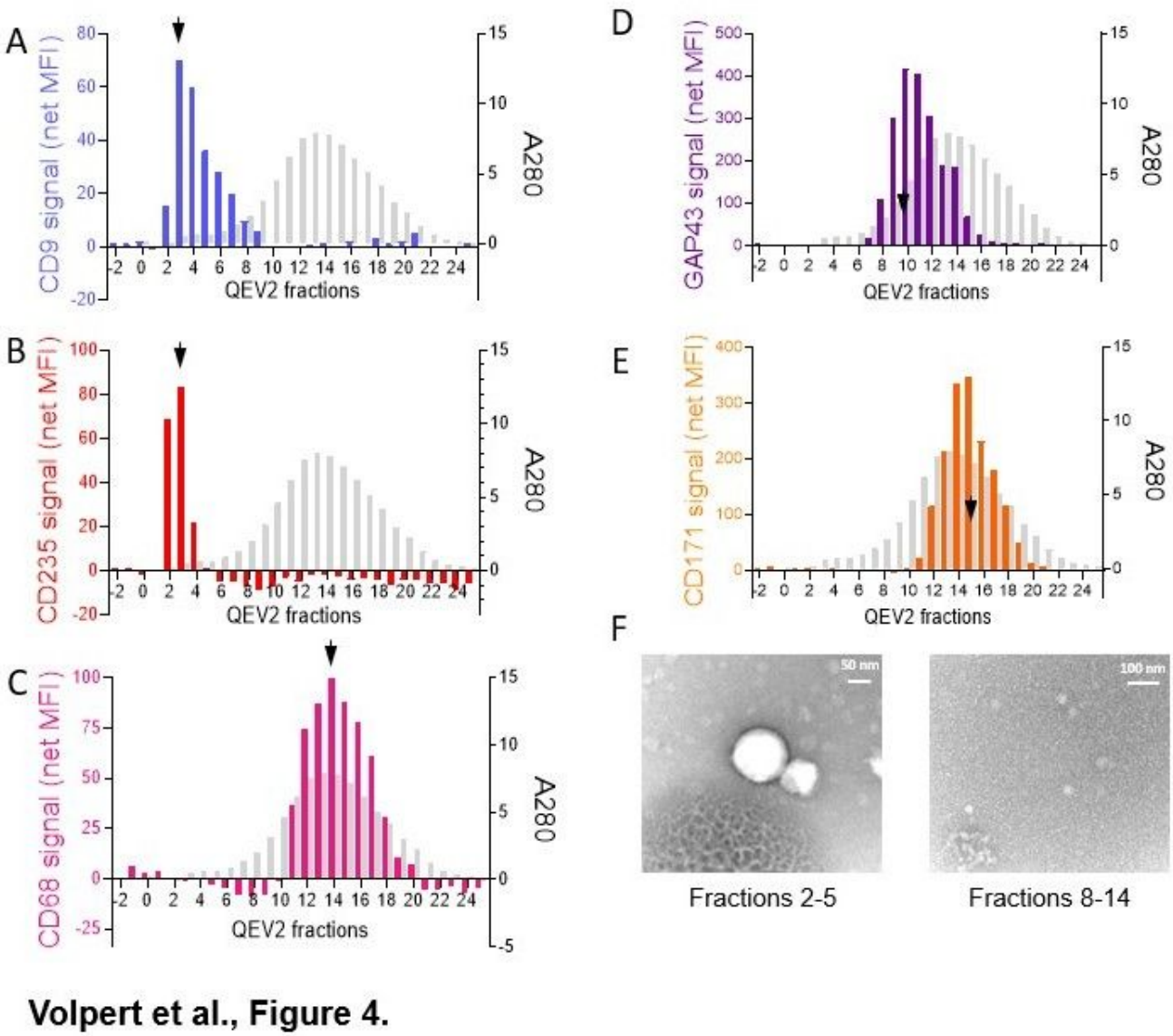

Figure 4

Lumin-EX reveals dramatic size differences between plasma EV populations positive for distinct cell-specific antigens. EV from 5 ml plasma, were enriched by PEG-based precipitation, resuspended in 2 ml PBS and loaded onto QEV2 35nm column (IZON Sciences). Two-ml fractions were collected following the manufacturer's protocol. Protein concentrations (A280) were measured in each fraction, including 3 void fractions (denoted -2, -1 and 0) and 50 ml aliquots analyzed by Lumin-EX. The fractions with the peak concentrations of specific EV (detected with pan-TSPN antibody cocktail) are indicated by arrows. **(A)** Lumin-EX with CD9 capture beads, combined with pan-TSPN detection. Eluted p is shown in grey. **(B)** Lumin-EX with capture beads against erythrocyte marker CD235 and pan-TSPN detection. **(C)** capture with the antibody against a macrophage marker, CD68, combined with pan-TSPN detection. **(D)** Lumin-EX capture with beads for axonal marker, GAP43, pan-TSPN detection. **(E)** ICD171 capture (neuronal marker), detection with pan-TSPN antibody cocktail. Note that CD9-positive and CD235 positive EV are collected in early fractions, consistent with the average diameter of 150-200 nm, EV positive for CD68, CD171 and GAP43 peak in later fractions, consistent with diameters of 30-50 nm and below. **(F)** Pooled, concentrated fractions 2-5 and 8-14 (qEV Original, IZON Sciences) were loaded onto microgrids, stained with aqueous uranyl acetate, and analyzed by transmission electron microscopy.

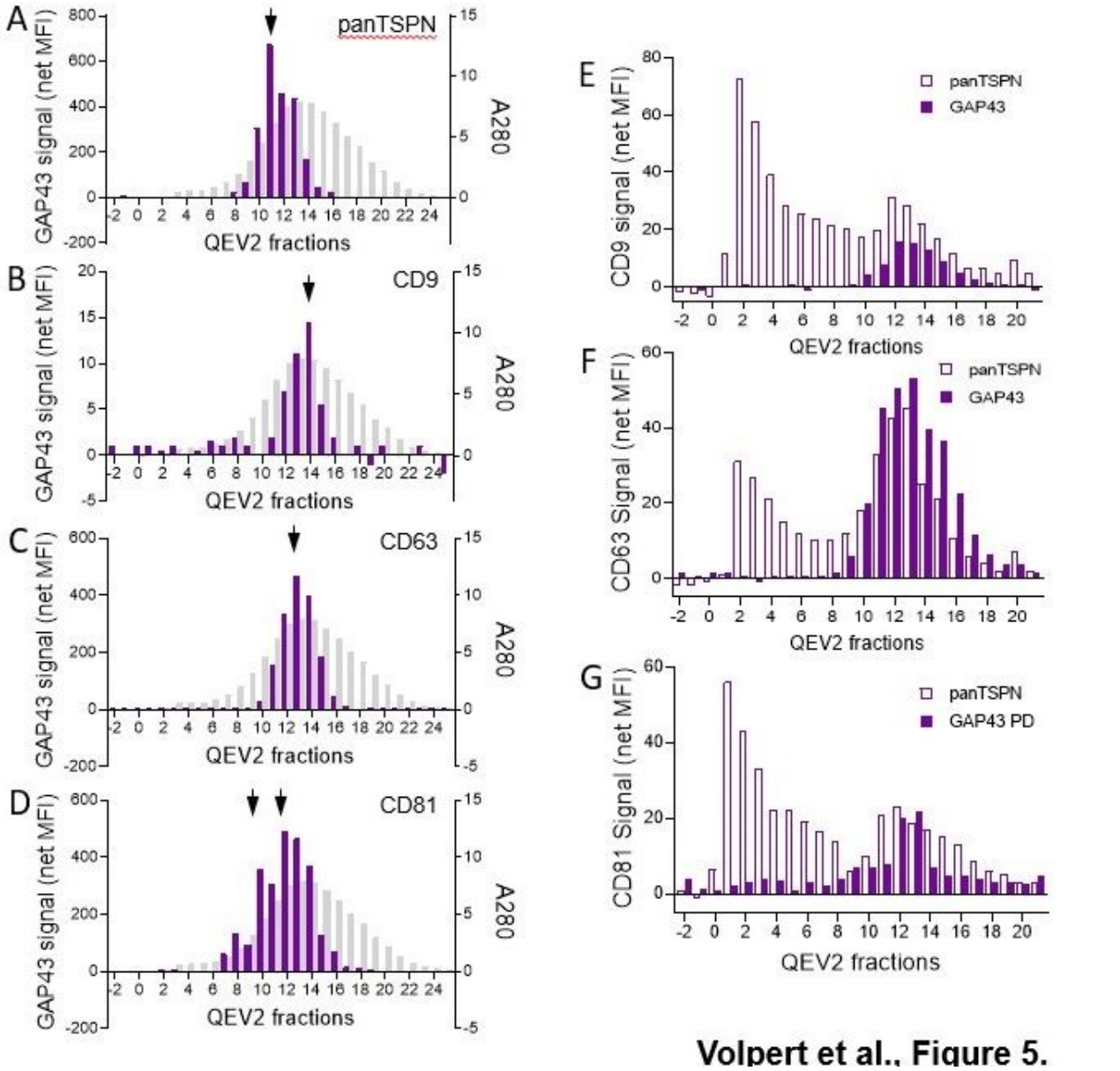

Figure 5

Intact EV Luminex reveals a continuum of sizes amongst tetraspanin-positive structures (EVs) in blood plasma. **(A-D)** Fractions collected from QEV2 column were subjected to IEL for axonal marker GAP43 and probed with the pan-TSPN antibody cocktail (A) or with the antibodies against CD8 (B), CD63 (C) and CD81 (D), respectively. Note that peak concentrations are observed in different fractions for distinct tetraspanins, covering a broad range of sizes. **(E-G)** QEV2 fractions were subjected to IEL for CD9 (E), CD63 (F) and CD81(G), and probed with antibodies against axonal marker, GAP43, or with pan-TSPN antibody cocktail, as shown. Note a broad range of sizes for all analytes and detection antibody combinations.

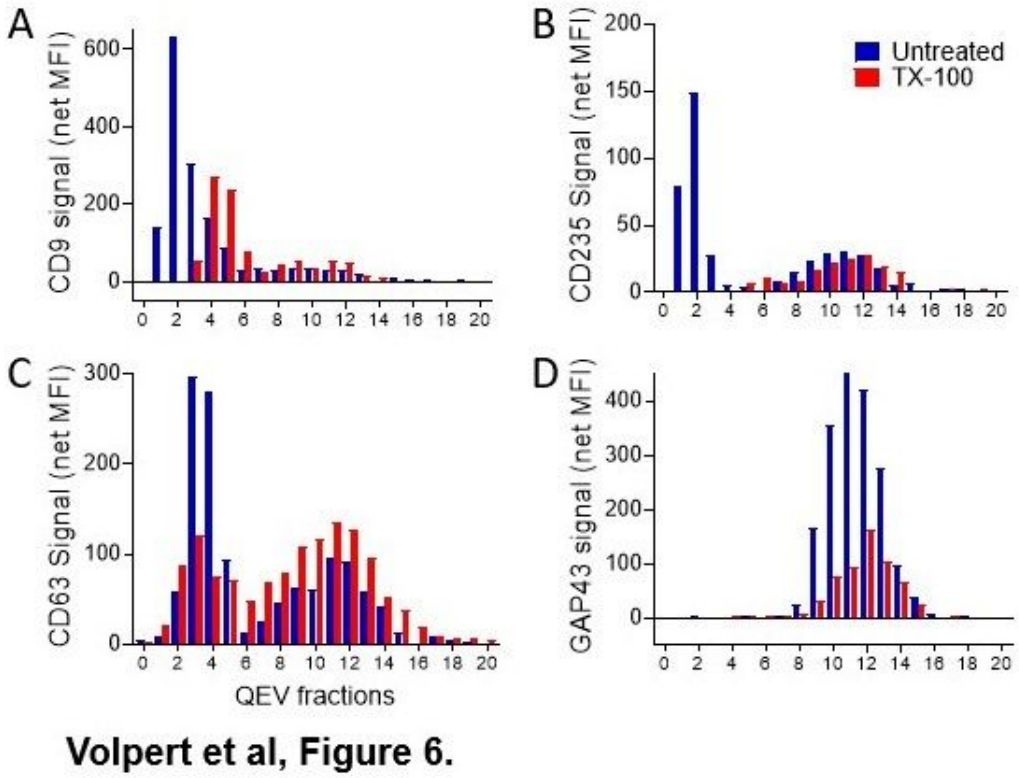

Figure 6

Plasma membrane disruption by Triton X-100 pre-treatment of plasma samples diminishes IEL signal. Plasma samples were concentrated by PEG-based precipitation, reconstituted in 1x PBS. The samples were then pre-treated with TX-100 (red bars) or sham buffer (blue bars) and subjected to size-exclusion chromatography (IZON qEV2 column). The fractions were then subjected to IEL with **(A)** CD9, **(B)** CD235, **(C)** CD63 and **(D)** GAP43 beads paired with pan-TSPN detection cocktail. Note diminished signal upon of TX-100 pre-treatment, for both early and late fractions.

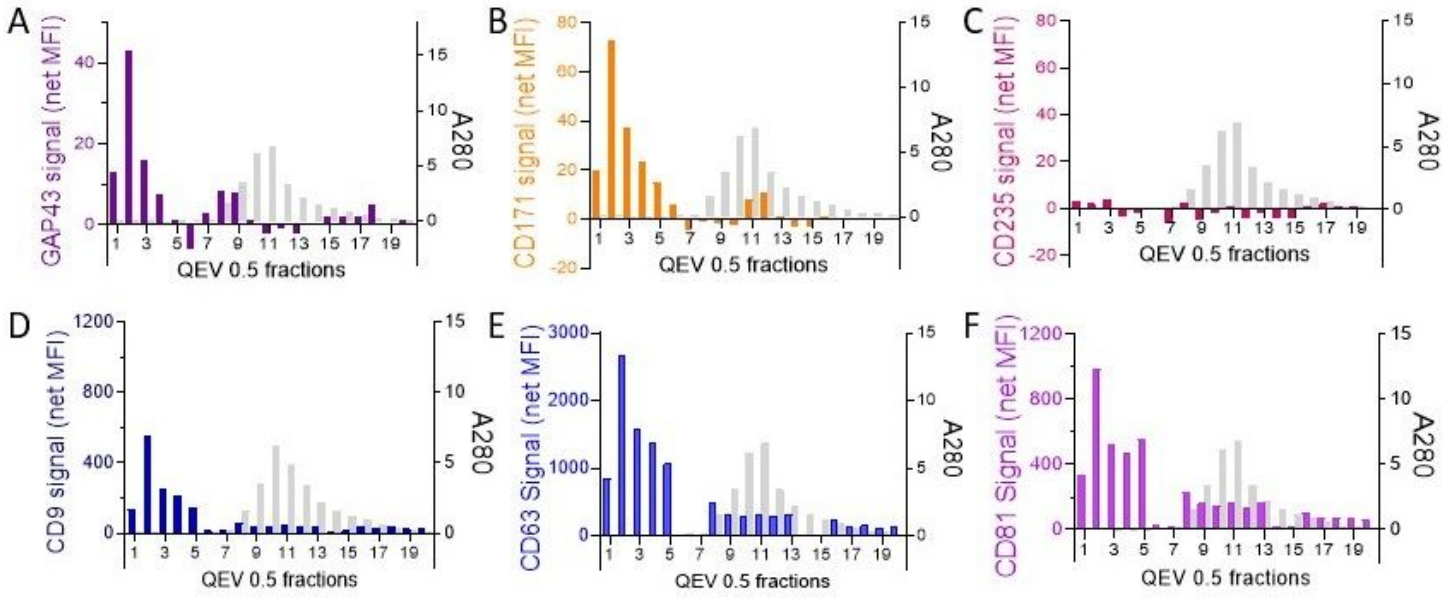

Figure 7

IEL analysis of neuronal cell conditioned media. Serum-free media conditioned by iPSC-derived neurons (BrainXell, 10 ml) was collected, cleared by filtration via Amicon spin filter (100 kDa MWCO) reconstituted in 0.5 ml PBS, and processed by SEC using QEV original column (35 nm, ZON Sciences). Fractions (0.5 ml) were collected according to the manufacturer's instructions and protein concentration (A280) determined in each fraction (gray bars). All fractions (1-20, 50 ml per sample) were subjected to IEL with beads for **(A)** GAP43, **(B)** CD171 and **(C)** CD235 followed by detection with pan-TSPN antibody cocktail. Note the lack of CD235-positive EVs in the media conditioned by iPSC neurons (specificity control). **(D-F)** IEL of the QEV fractions with beads for EV markers, CD9 (D), CD63 (E) and CD81 (F). Note for each marker, except CD235, a secondary smaller peak or disperse signal in the late fractions.

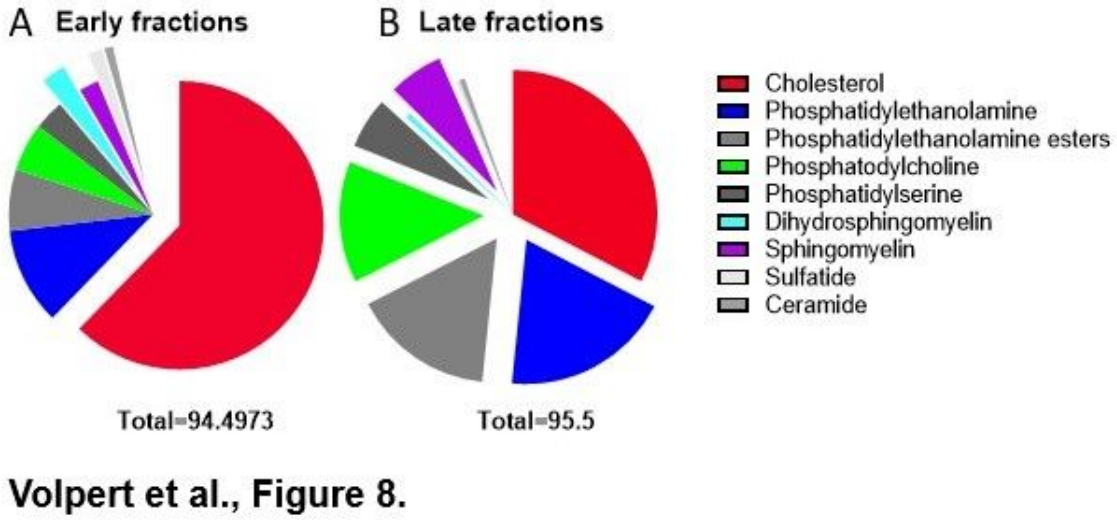

Figure 8

Lipid composition of late and early SEC fractions. Plasma EVs were concentrated as described in Methods and processed by SEC (qEV2, IZON, Sciences). Fractions 2-5 and 8-13 were pooled, concentrated using Amicon spin filter (100kDA MWCO) and subjected to lipidomic analysis (see Methods). Each fraction was analyzed in biological triplicate. The pie charts show proportional contribution (% of total lipid) for the indicated specific lipid classes in the early **(A)** and late fractions **(B)** is shown. “Exploding” sectors indicate lipids with higher proportional content. For minor lipid constituents (average content in early fractions < 0.1%), see Table 5.

Supplementary Files

This is a list of supplementary files associated with this preprint. Click to download.

- SupplementaryData.docx